Morphology-Dependent Trap Formation in High Performance Polymer Bulk Heterojunction Solar Cells

*Zach M. Beiley, Eric T. Hoke, Rodrigo Noriega, Javier Dacuña, George F. Burkhard, Jonathan A. Bartelt, Alberto Salleo, Michael F. Toney, and Michael D. McGehee**

Bulk heterojunction solar cells (BHJs) based on poly[N-9′′-hepta-decanyl-2,7-carbazole-*alt*-5,5-(4′,7′-di-2-thienyl-2′,1′,3′-benzothiadiazole)] (PCDTBT) can have internal quantum efficiencies approaching 100% but require active layers that are too thin to absorb more than ~70% of the above band gap light. When the active layer thickness is increased so that the cell absorbs more light, the fill factor and open circuit voltage decrease rapidly, so that the overall power conversion efficiency decreases. We find that hole-traps in the polymer, which we characterize using space-charge limited current measurements, play an important role in the performance of PCDTBT-based BHJs and may limit the active layer thickness. Recombination due to carrier trapping is not often considered in BHJs because it is not believed to be a dominant loss mechanism in the "fruit-fly" P3HT system. Furthermore, we show that in contrast to P3HT, PCDTBT has only weak short-range molecular order, and that annealing at temperatures above the glass transition decreases the order in the π–π stacking. The decrease in structural order is matched by the movement of hole-traps deeper into the band gap, so that thermal annealing worsens hole transport in the polymer and reduces the efficiency of PCDTBT-based BHJs. These findings suggest that P3HT is not prototypical of the new class of high efficiency polymers, and that further improvement of BHJ efficiencies will necessitate the study of high efficiency polymers with low structural order.

1. Introduction

Bulk heterojunction solar cells (BHJs) made from blends of poly(3-hexylthiophene) (P3HT) and [6,6]-phenyl-C61-butyric acid methyl ester (PCBM) are frequently referred to as the "fruit-fly" of BHJs[1] because they are extensively studied as a model system. Though in the past they were considered a high efficiency system with a typical power conversion efficiency of ~4.5%,[2] in recent years they have been surpassed in efficiency by devices made from a number of other polymers.[2–8] One of the most interesting of these polymers is poly[N-9′′-hepta-decanyl-2,7-carbazole-*alt*-5,5-(4′,7′-di-2-thienyl-2′,1′,3′-benzothiadiazole)] (PCDTBT), because BHJs made from it can have power conversion efficiencies above 7%,[9] internal quantum efficiencies approaching 100%,[10] and operating lifetimes exceeding 6 years.[11] Achieving this high power conversion efficiency and near perfect charge collection, however, requires active layers that are too thin (~70 nm) to absorb more than ~70% of the above band gap light.[10] By contrast, BHJs from P3HT/PCBM can be made optically thick, but do not surpass ~80% internal quantum efficiency, even in very thin devices.[12] Additionally, P3HT/PCBM BHJs require thermal annealing to achieve their highest efficiency,[13] while BHJs based on PCDTBT are best in an unannealed state.

In this work we demonstrate using X-ray diffraction and charge transport measurements that P3HT and PCDTBT differ widely in both morphology and electronic defect structure, and that this accounts for the differences in optimal BHJ active layer thickness and processing conditions. We show that in contrast to P3HT, which is a semi-crystalline polymer, PCDTBT has only weak, short-range molecular order. In P3HT, thermal annealing encourages crystallite growth and increases structural order, while in PCDTBT thermal annealing reduces the coherence length of the π–π stacking, increasing the disorder in the polymer's electronic structure. To account for

Z. M. Beiley, J. A. Bartelt, Prof. A. Salleo, Prof. M. D. McGehee
Department of Materials Science and Engineering
Stanford University
Stanford, CA 94305, USA
E-mail: mmcgehee@stanford.edu
E. T. Hoke, R. Noriega, Dr. G. F. Burkhard
Department of Applied Physics
Stanford University
Stanford, CA 94305, USA
J. Dacuña
Department of Electrical Engineering
Stanford University
Stanford, CA 94305, USA
Dr. M. F. Toney
Stanford Synchrotron Radiation Lightsource
SLAC National Accelerator Laboratory
Menlo Park, CA 94025, USA

DOI: 10.1002/aenm.201100204

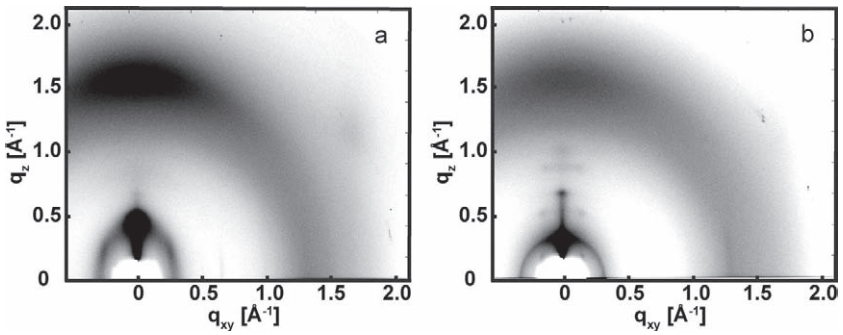

Figure 1. GIXS images of pure PCDTBT films (a) unannealed and (b) annealed at 200 °C for 10 minutes.

the high degree of disorder in PCDTBT films when describing hole transport, we have used a model of space-charge limited current that incorporates a distribution of traps extending into the band gap. A model that assumes an exponential distribution of traps successfully predicts hole-only currents over a wide range of voltages, temperatures and film thicknesses. Lastly, by using thermal annealing as a tool to control the trap distribution in PCDTBT, we show that photocurrent collection in PCDTBT-based BHJs is dependent on the distribution of hole-traps in the polymer. This suggests that the presence of traps limits PCDTBT-based BHJs to optimal thicknesses that are too thin to absorb all of the above band gap light.

2. Results and Discussion

2.1. PCDTBT Morphology

To characterize the morphology of PCDTBT films we have performed grazing incidence X-ray scattering (GIXS) measurements at the Stanford Synchrotron Radiation Lightsouce on as-cast and annealed films (**Figure 1**). We attribute the prominent peak at $q \approx 1.58$ Å^{-1} ($d \approx 4.0$ Å) to the π–π stacking of the polymer, which is primarily oriented out of the plane of the substrate (face-on packing), though the smearing of the peak into a ring indicates that there is a distribution of π–π stacking orientations. There are a few other peaks which we attribute to lamellar and backbone spacings of the polymer, however the low number and intensity of these peaks indicates that the polymer has only weak short-range order, consistent with previous reports[14] of PCDTBT morphology. This contrasts with P3HT, for which even unannealed films are significantly crystalline, resulting in multiple peaks in the GIXS pattern.[15] Upon annealing PCDTBT films to 200 °C, a few more peaks emerge along the meridian of the GIXS pattern ($q \approx q_z$ at 0.88 Å^{-1} and 1.10 Å^{-1}), which we attribute to additional lamellar and backbone spacings, indicating a small increase in the crystallinity of the film. The π–π stacking direction remains primarily oriented out of the plane of the substrate at $q \approx 1.58$ Å^{-1} (**Figure 2**), with a spread of orientations similar to that of the unannealed film.

The full width at half maximum (FWHM) of the scattering peaks, Δq, gives an estimation of the length over which ordered crystalline packing is maintained,[15] known as the coherence length, by the relation $L_{coh} = 2\pi/\Delta q$. Figure 2 shows cake segments extracted from GIXS images through the π–π stacking peaks along the meridian ($q_{xy} \approx 0$) for films annealed for 10 minutes at different temperatures. For annealing temperatures above the glass transition ($T_g \approx 130$ °C),[16] the π–π stacking peak broadens and the coherence length decreases. The asymmetry in the peak broadening upon annealing is due to the emergence of a second broad peak at $q \approx 1.3$ Å^{-1}, which we speculate may be due to an increase in the density of locally ordered side-chains. By fitting the data to two independent pseudo-Voigt peaks, we find that that the coherence length of the π–π stacking peak decreases from 13.4 Å in the unannealed film to 10.1 Å in the film annealed at 200 °C (**Figure 3**). This indicates that thermal annealing causes the polymer's π–π stacking to become more disordered, a stark contrast to P3HT, in which annealing causes an increase in the coherence length due to the growth of crystallites.[15,17]

The finding that thermal annealing decreases the coherence of PCDTBT π–π stacking is notable because it is often assumed that thermal annealing always increases the crystallinity of polymers. In P3HT, a polymer packing motif exists that allows simultaneously for dense π–π and side-chain packing, and thermal annealing causes P3HT to move toward this structure.[18] In PCDTBT there may be no ordered packing motif that gives dense packing of both the π–π stacking and the side chains at the same time due to the shape and chemical structure of the monomer (Figure 2). In this case the polymer conformation must favor dense packing of either the side chains or the π–π stacking. We propose that in PCDTBT the driving

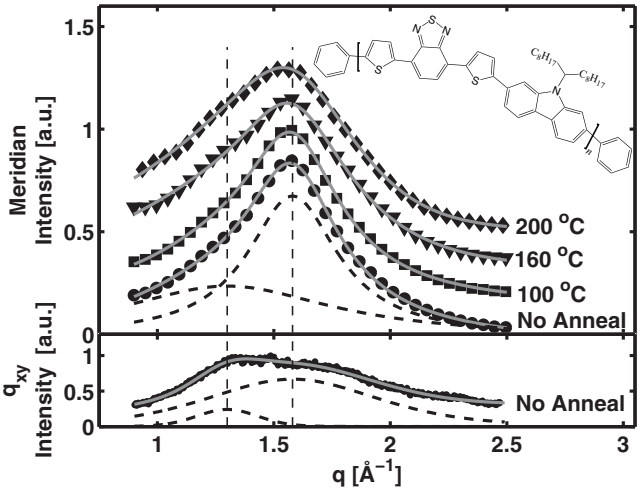

Figure 2. Top panel: cake segments (symbols) through GIXS images along the meridian ($q_{xy} \approx 0$) for PCDTBT films thermally annealed for 10 minutes at different temperatures. Bottom panel: line cut along q_{xy} ($q_z = 0.02$ Å^{-1}) for the unannealed PCDTBT film, showing a prominent peak at $q = 1.3$ Å^{-1}, which also has some component in the q_z direction. The solid gray lines show fits to superpositions of two pseudo-Voigt peaks centered at $q = 1.3$ Å^{-1} and $q = 1.58$ Å^{-1} (marked by vertical dashes) and the dashed lines show the decomposed peaks for the unannealed sample. The inset shows the chemical structure of PCDTBT.

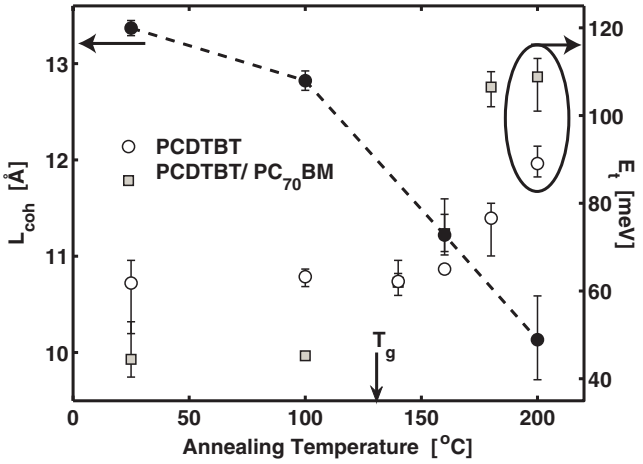

Figure 3. Left axis: The coherence length of the π–π stacking for thermally annealed PCDTBT films (Figure 2). The error bars represent the standard error of the best-fit values. Right axis: The width of the exponential trap distribution for pure PCDTBT and 1:4 PCDTBT: $PC_{70}BM$ films as a function of annealing temperature. The error bars represent the range of values obtained from several devices. The points at 25 °C correspond to unannealed samples.

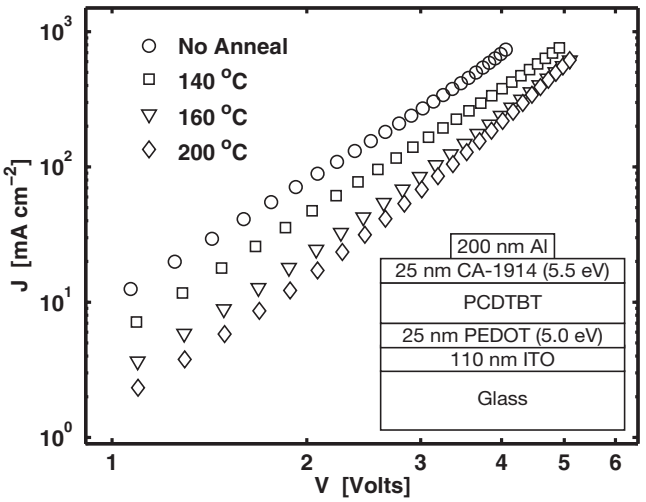

Figure 4. Room temperature current vs. voltage on a log-log plot for pure PCDTBT hole-only devices annealed at different temperatures. The device active layers are all ~100 nm in thickness. The inset shows a schematic of the device architecture.

force for side chain agglomeration dominates that for densification of the π–π stacking. Thus upon thermal annealing, the side chains become better packed at the expense of the order in the π–π stacking direction, resulting in a decrease in the π–π stacking coherence length.

2.2. Hole Transport Characteristics

The structural order of the π–π stacking is an important factor in determining the electronic structure of polymers, and is known to correlate directly with charge carrier mobility[19,20] and localization in trap states.[21] To characterize hole transport in PCDTBT, we have performed space-charge limited current measurements on hole-only devices using the device architecture that is shown schematically in the inset of **Figure 4**. In our hole-only devices, PEDOT (Clevios P VP AI 4083, ~5.0 eV) is used as the hole injecting contact and CA-1914 (Plextronics, ~5.5 eV), a proprietary conducting polymer with a functionality similar to that of PEDOT, is used as the hole extracting (electron blocking) contact. We used CA-1914, instead of gold or palladium, as a top contact to avoid evaporating metal directly on the active layer, and we performed annealing before depositing the CA-1914 and aluminum layers to avoid any reaction that may occur at the active layer/electrode interface at elevated temperatures. Figure 4 shows on a log-log plot the room temperature currents vs. voltage for hole-only devices that were annealed for 10 minutes at different temperatures. In the range of measured voltages, the current decreases with increasing annealing temperature indicating that hole transport becomes worse with thermal annealing. By contrast, thermal annealing improves hole transport in P3HT and many other polymers.[13,22] A previous study[14] of charge transport in PCDTBT field effect transistors found a slight increase in hole mobility for annealing temperatures in this range. However the transistor geometry measures current in the in-plane direction and is highly dependent on the polymer-dielectric interface, so that our observation of a decrease in out-of-plane mobility with thermal annealing is not necessarily inconsistent with this study.

We have applied several space-charge limited current models to hole-only currents over a range of voltages and temperatures, taken for PCDTBT devices of different thicknesses. Hole-only currents in disordered organic semiconductors, including P3HT, are commonly modeled using analogues of Child's Law,[23] which describes single carrier currents in a trap-free insulator and predicts that the current density (J) varies by the square of the applied bias (V) and inversely by the cube of the film thickness (L) according to Equation (1).

$$J = \frac{9}{8}\varepsilon\mu_h\frac{V^2}{L^3} \quad (1)$$

Here ε is the dielectric constant of the material and μ_h is the hole mobility, which is assumed to be constant. The hole-only currents in PCDTBT devices, however, exhibit very strong dependences on voltage ($J \sim V^{3.5}$) and active layer thickness, ($J \sim L^{-6}$), which are very different from the dependences predicted by Child's Law. In an attempt to resolve these discrepancies, we have considered several modifications to Child's Law, which incorporate a variable charge carrier mobility and are commonly used to describe hole transport in disordered organic semiconductors. The variable mobility in these models is due to a distribution of transport states in energy, or energetic disorder, which causes the mobility to increase with increasing applied electric field,[24,25] or with increasing injected carrier density,[26] or both. In these models increasing the film thickness reduces the mobility enhancement and the model converges with Child's Law, however the hole-only currents in PCDTBT devices obey a power law in voltage that does not change with film thickness for films ranging from 100–500 nm.

Because of this, these commonly used space-charge limited current models are not appropriate for describing hole transport in PCDTBT films. Additionally, the power law dependence of the current on voltage and the strong thickness dependence rule out the possibility that the current is injection limited, since Fowler-Nordheim tunneling predicts an exponential voltage dependence and a much weaker thickness dependence ($J \sim L^{-2}$),[27] even though the nominal polymer HOMO[10] (–5.5 eV) implies a small barrier for hole injection from the PEDOT.

The current vs. voltage characteristics of the hole-only PCDTBT devices are successfully described by a model[28] of space charge limited current that incorporates an exponential distribution of traps. The distribution of states assumed in the model is given as a function of energy (E) by Equation (2), where N_t is the total density of trap states in the distribution, E_t is the characteristic width of the distribution in energy, and E_{HOMO} is the edge of a band of transport states with an effective density N_{HOMO}.

$$D_t(E) = \frac{N_t}{E_t} \exp\left(\frac{E_{HOMO} - E}{E_t}\right) \quad (2)$$

This distribution of states is schematically illustrated in **Figure 5**, which shows a long exponential tail extending away from a relatively narrow band of transport states. This model was first proposed in 1962 by Mark and Helfrich to describe hole transport in organic crystals.[28] It has been frequently used to describe electron,[29–34] and somewhat less often hole,[35–37] transport in conjugated polymers. The model assumes that carriers lying deeper in the band gap than the Fermi level are "deeply" trapped and have zero mobility. Mobile carriers, whose density is determined by thermodynamic equilibrium according to the Boltzmann distribution, hop in the transport states with a mobility μ_h.

The analytical form of the model is given by:

$$J = q\mu_h N_{HOMO} \left(\frac{\varepsilon}{q N_t} \frac{m}{m+1}\right)^m \left(\frac{2m+1}{m+1}\right)^{m+1} \frac{V^{m+1}}{L^{2m+1}} \quad (3)$$

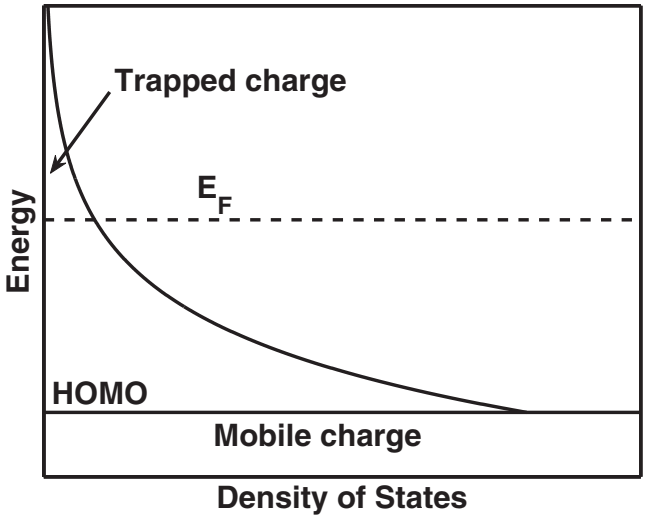

Figure 5. Schematic representation of the exponential trap distribution in PCDTBT along with a band of transport states in the HOMO. Charge deeper in the gap than the Fermi level (E_F) is considered deeply trapped, and has zero mobility.

where q is the electron charge and

$$m = \frac{E_t}{kT} \quad (4)$$

All other variables are as described above. The model predicts that the current varies with voltage according to a power law ($m + 1$) that is determined by the temperature and the characteristic width of the trap distribution. Thus measuring the slope on a log-log plot of the hole-only current vs. voltage allows the rapid characterization of the width of the trap distribution in energy. The width of the trap distribution also determines the dependence of current on film thickness, $J \sim L^{-(2m+1)}$, which is very strong since m frequently ranges from 2–4. Although the magnitude of the current varies with film thickness, the voltage power law does not, which sets this model apart from many models of space-charge limited current that incorporate a variable mobility.

This model successfully predicts the current in PCDTBT hole-only devices over a wide range of voltages, temperatures and film thicknesses. **Figure 6**a shows hole-only currents for a single device with an active layer thickness of 237 nm and best fits to Equation (3). The fits were performed using 3 fitting parameters for currents obtained over the entire range of temperatures: $\mu_h N_{HOMO}$ (the hole mobility multiplied by the effective density of states of the transport band), E_t and N_t. Figure 6b shows hole-only currents for four devices of different film thicknesses and best fits to Equation (3) where, as above, only 3 fitting parameters were used over the entire range of voltages, temperatures and film thicknesses. The best fit parameters that characterize hole-only currents in as-cast PCDTBT films are E_t = 60 meV, $\mu_h N_{HOMO} = 2.4 \times 10^{15}$ $(cmVs)^{-1}$ and $N_t = 4.7 \times 10^{17}$ cm^{-3}. These best-fit parameters are slightly different from those found for fits to any single device (Figure 6a) due to the intrinsic variability of devices.

The best-fit value for $\mu_h N_{HOMO}$ has good physical significance. We measured the room temperature hole mobility by photo-CELIV[38,39] to be ~6×10^{-5} cm^2 V^{-1} s^{-1}. Dividing the extracted value $\mu_h N_{HOMO} = 2.4 \times 10^{15}$ $(cmVs)^{-1}$ by the photo-CELIV mobility gives $N_{HOMO} \approx 4 \times 10^{19}$ cm^{-3}, which is similar to values[40] commonly assumed for the effective density of HOMO states. At the same time, the best-fit value for N_t is too small to have good physical significance. The model assumes that the trapped carrier density is much larger than the free carrier density, however in the range of voltages and film thicknesses measured, a total trap density of ~5×10^{17} cm^{-3} means that the free and trapped carrier populations are of a similar size.[23] There are several reasons, however, that the best-fit value for N_t may be smaller than the true density of traps in the band gap, all of which stem from temperature dependences that are not included in the analytical model given in Equation (3). The model assumes that mobility and effective density of states are independent of temperature, which may not be good assumptions given the hopping nature of hole transport in disordered organic semiconductors.[30] Including these temperature dependences in the model, as has been done for PPV-based polymers by Mandoc et al.,[30] leads to an increase in the best-fit value for N_t. The model also does not account for a temperature dependent transport energy[41] (E_{HOMO}), which would manifest itself in a temperature dependent N_{HOMO}. Refining the model to include these temperature dependences

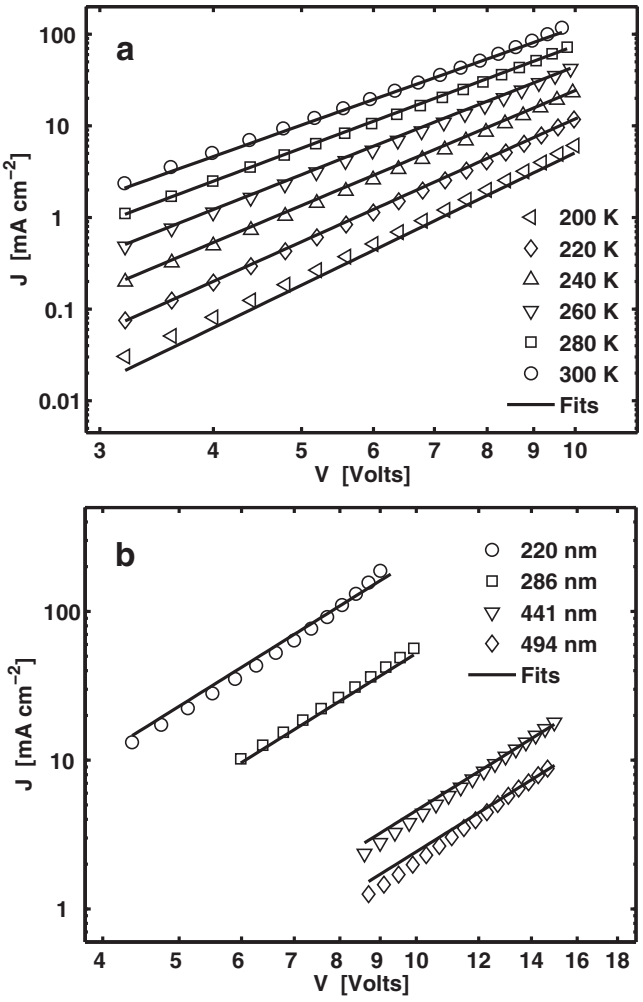

Figure 6. Current vs. voltage data and curve fits to Equation (3) for PCDTBT hole-only devices. a) Currents for a single device (L = 237 nm) over a range of temperatures, using best-fit parameters $\mu_h N_{HOMO} = 1.4 \times 10^{15}$ (cmVs)$^{-1}$, $E_t = 65.6$ meV and $N_t = 3.3 \times 10^{17}$ cm^{-3}. (b) Room temperature currents for devices of different thicknesses using best-fit parameters $\mu_h N_{HOMO} = 2.4 \times 10^{15}$ (cmVs)$^{-1}$, $E_t = 60$ meV and $N_t = 4.7 \times 10^{17}$ cm^{-3}.

will change the values of N_t and N_{HOMO} that are extracted from curve fits, but will not alter either the voltage or film thickness dependences of the analytical model in Equation (3). Since the value of E_t is determined directly from the voltage dependence of the measurement, we argue that the simple analytical model captures all the essential physics for evaluating trends in the width of the trap distribution in PCDTBT hole-only devices. The remarkably close agreement of the model given in Equation (3) with the observed voltage, temperature and thickness dependences strongly suggests that space-charge limited hole currents in PCDTBT are dominated by a high density of hole-traps.

2.3. Hole-Traps and PCDTBT Morphology

While the magnitude of the current decreases in PCDTBT films upon thermal annealing, the voltage power law increases (Figure 4). According to Equation (3) an increase in voltage power law is due to an increase in E_t, which implies a broadening of the trap distribution in energy. Figure 3 shows the values of E_t, which were extracted from fits of hole-only currents to Equation (3), as a function of annealing temperature. In pure PCDTBT films, the trap distribution widens significantly for annealing temperatures above T_g, increasing from ~62 meV for unannealed films to ~89 meV for films annealed at 200 °C, an increase of ~44%. For annealing temperatures below T_g there is essentially no difference when compared with unannealed devices.

The measured increase in the energetic width of the trap distribution upon thermal annealing of PCDTBT films corresponds well with the increase in structural disorder, as measured by GIXS. The films used for GIXS measurements were prepared the same way and measured over the same annealing temperatures as those used in hole-only devices. The close correspondence of structural and energetic disorder suggests that the traps in PCDTBT are related to the packing order in the polymer. It is known that the degree of interchain π–π orbital overlap is partly responsible for determining the HOMO energy,[42] and that a greater degree of disorder in π–π orbital overlap results in a greater spread of HOMO energies[43] and an increased breadth of the sub-band gap tail states.[21] That the energetic spread in electronic states corresponds with the physical spread in π–π stacking spacings suggests that the hole-traps in PCDTBT may be very deep HOMO states, and not a unique chemical species formed by impurities in the film or by photo-oxidation of the polymer. This conclusion is supported by the recent finding of remarkable stability for PCDTBT transistors in air.[14]

PCDTBT-based BHJ solar cells are typically made by blending PCDTBT with $PC_{70}BM$ in a 1:4 weight ratio. To investigate the effects of blending with $PC_{70}BM$ on hole transport in PCDTBT, we fabricated hole-only devices of 1:4 PCDTBT: $PC_{70}BM$ blend films (PCDTBT/$PC_{70}BM$). The same device architecture was used for hole-only measurements on PCDTBT/$PC_{70}BM$ blends as on pure PCDTBT films. The use of high work function electrodes (5.0–5.5 eV) in these devices rules out contributions from both electron and hole currents in $PC_{70}BM$, so that the differences in current between pure and blend devices can be attributed entirely to changes in the hole transport characteristics of PCDTBT. Figure 3 shows that films composed of PCDTBT/$PC_{70}BM$ blends have a narrower trap distribution with a width of ~44 meV, compared with ~62 meV in pure PCDTBT films. A similar trend with thermal annealing was seen for the width of the hole-trap distribution in PCDTBT/$PC_{70}BM$ blends as for pure PCDTBT. Although GIXS measurements were made on PCDTBT/$PC_{70}BM$ blends, the weak π–π stacking peak in PCDTBT could not be resolved due to the presence of strong scattering from $PC_{70}BM$ crystallites at overlapping q values. However, since the energetic disorder correlates with structural disorder in pure PCDTBT films, we infer that the decrease in energetic disorder in PCDTBT upon blending with PCBM is due to an increase in structural order. This is different from what has been observed in P3HT/PCBM blends, in which the intimate mixing of P3HT and PCBM disrupts P3HT crystal formation,[15,44] resulting in a decrease in hole mobility.[13] The ordering effect that $PC_{70}BM$ has on PCDTBT may be by a mechanism similar to that observed in blends of

MDMO-PPV,[45–47] whereby interactions between the polymer and PCBM molecules causes the polymer to uncoil into a morphology that is more favorable for hole transport.

2.4. PCDTBT/$PC_{70}BM$ Solar Cell Performance

The processing parameters that make optimal PCDTBT-based BHJs are very different from those that make optimal P3HT-based BHJs. Solar cells made with P3HT/PCBM are optimal in a 1:1 blend ratio, when films are optically thick (>200 nm). The fill factor and open circuit voltage are roughly independent of film thickness because the carrier mobilities and lifetimes are large enough that even a small electric field can extract most of the charge carriers in optically thick films.[13] Charge carrier recombination in P3HT/PCBM BHJs has been attributed to geminate[13] and bimolecular[48] (Langevin) recombination, and is significant enough that the internal quantum efficiency does not surpass ~80%.[12] This behavior is very different from that observed in PCDTBT solar cells, in which the optimal blend ratio is 1:4, and in which the internal quantum efficiency can approach 100%, though the active layer must be so thin as to absorb only ~70% of the incident above band gap light.[10] The power conversion efficiency reported by Park et al.[10] for the device with near 100% internal quantum efficiency was 6.1%, and was achieved using a TiO_x spacer layer between the active layer and the reflective back electrode to optimize the optical interference for maximum absorption. We have matched the efficiency of that device, though our device architecture does not employ an optical spacer. The current vs. voltage curve and the figures of merit for this solar cell are shown in **Figure 7**. When the active layer thickness is increased beyond ~70 nm so that the cell absorbs more light, the fill factor and open circuit voltage decrease rapidly, so that the overall power conversion efficiency decreases. We propose that the reason for the rapid decrease in power conversion efficiency when the cells are made thicker than is optimal is increased recombination due to hole-traps.

Recent work on PCDTBT/$PC_{70}BM$ BHJs has suggested that recombination occurs through traps located at the PCDTBT/$PC_{70}BM$ interface.[49,50] Street et al.[49] looked at the voltage and temperature dependence of photocurrent collection in PCDTBT/$PC_{70}BM$ solar cells and concluded that they are inconsistent with commonly accepted models of geminate and bimolecular recombination. As a result they concluded that traps mediate recombination through a Shockley-Read-Hall (SRH) type mechanism, which has been largely ruled-out in other polymer-fullerene BHJs. Though the method by which they reached their conclusion has been disputed,[51,52] there has since been other work[50,53] to support the notion of trap mediated recombination in PCDTBT-based BHJs.

In order to probe the effect of the hole-trap distribution on PCDTBT/$PC_{70}BM$ BHJ performance, we made optically thick (~250 nm active layers) solar cells annealed at different temperatures up to 200 °C. We studied thicker than optimal PCDTBT/$PC_{70}BM$ BHJs to magnify the effects of recombination, since optimal cells have near-perfect charge collection efficiency, although our findings were similar for thick and thin devices. As discussed above, thermal annealing causes the hole-traps to become more widely distributed in energy (Figure 3). Because the distribution is exponential, as the width of the distribution increases, so does the energetic depth of the average trap, which means that thermal annealing in effect causes the traps to move deeper into the band gap.

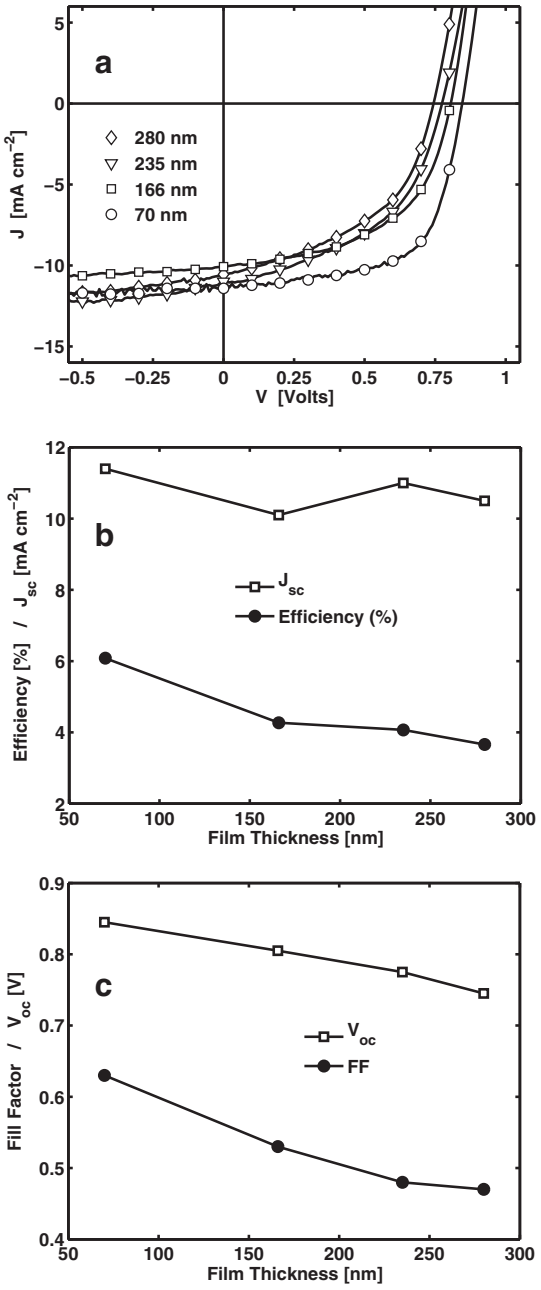

Figure 7. Unannealed PCDTBT/$PC_{70}BM$ solar cell (a) current vs. voltage and (b and c) figures of merit for different active layer thicknesses.

Figure 8 shows the effects of thermal annealing on the performance of thick PCDTBT/$PC_{70}BM$ BHJs. The external quantum efficiency (Figure 8a) was measured as a function of applied voltage using a low-intensity monochromatic light (λ = 500 nm), which was chopped at 200 Hz and superimposed on a

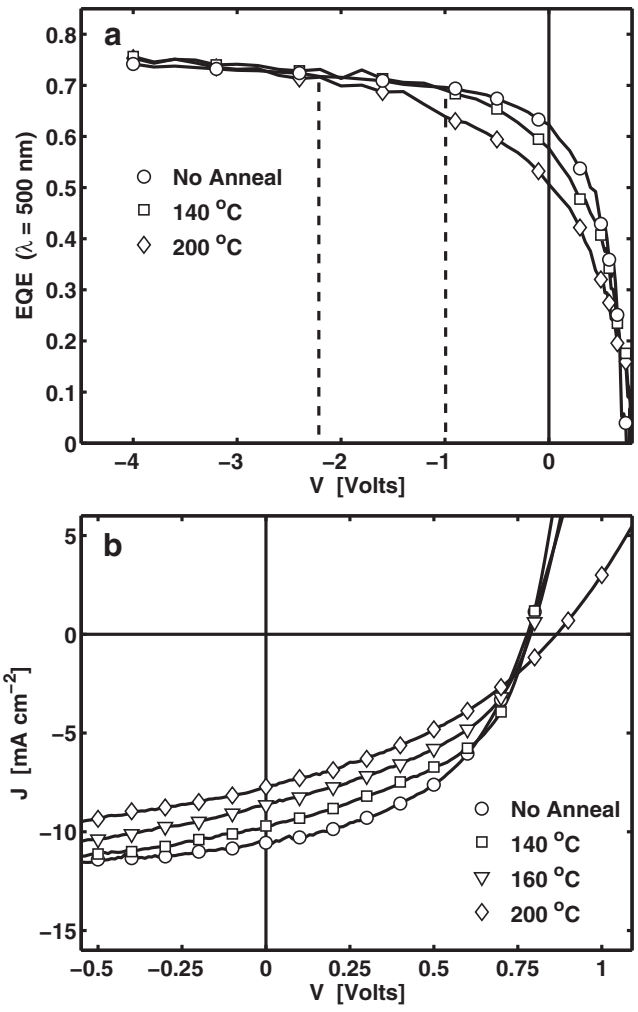

Figure 8. PCDTBT/$PC_{70}BM$ solar cell (a) external quantum efficiency (λ = 500 nm) vs. voltage and (b) current vs. voltage for different annealing temperatures. The devices are all ~250 nm thick.

1 sun white light bias to mitigate the effects of photoconductivity when large negative voltages were applied.[54] There are two important trends to notice from this measurement. The first is that as the traps move deeper into the band gap with increasing annealing temperature, the solar cells require larger reverse biases to achieve equivalent charge collection efficiency. The larger density of deep traps in annealed cells means that carrier lifetimes are lower compared with those in unannealed cells. The carrier lifetimes may be reduced either by trap-mediated recombination, as suggested by Street et al., or by the formation of space-charge in deep traps, which reduces the internal electric field that drives charge separation. In either case, the result is that devices with deeper traps require stronger biases to extract an equivalent photocurrent (Figure 8a) and have lower fill factors (Figure 8b).

The second interesting feature of Figure 8 is that, for sufficiently large reverse biases, annealed cells produce equivalent photocurrent to unannealed cells. This indicates that no excitons are lost due to morphology coarsening, as has been reported for BHJs made from other polymers.[46,55] The apparent absence of morphology coarsening can be explained by the formation of an intercalated structure in polymer-fullerene blends,[46] like that formed by fullerenes and thiophene-based polymers with sufficiently large side-chain spacings.[56–58] Furthermore, BHJs made with PCDTBT are optimal in a 1:4 blend ratio, which is suggestive of the formation of an intercalated structure, whereas P3HT-based BHJs are optimal in a 1:1 ratio,[2] and it is known that the side chains in P3HT are too closely spaced to allow PCBM to intercalate.[56] To support the claim that PCBM molecules intercalate with the PCDTBT side chains in a way that prevents morphological coarsening, we have performed photoluminescence (PL) quenching experiments on annealed and unannealed films of pure PCDTBT and PCDTBT/$PC_{70}BM$ blends. PL quenching fractions were calculated by dividing the spectrally integrated PL intensity of the blend film, corrected for difference in absorption between films, by that of a pure polymer film processed in an identical manner. We observed that for annealing temperatures ranging from 100 °C–200 °C and times ranging from 10 min.–60 min., all films exhibited >99.9% PL quenching. This indicates that even with extensive thermal annealing, there is not a significant degree of morphological coarsening such that polymer domains become larger than the exciton diffusion length. As a result, we attribute the change in solar cell performance upon annealing to the movement of traps deeper into the band gap.

3. Conclusions

The morphological findings presented here for PCDTBT run counter to the conventional wisdom gained from studying P3HT, implying that the morphology and device physics of P3HT may not serve as a good model for newer high efficiency systems. P3HT is semi-crystalline with its π–π stacking direction oriented parallel to the substrate. Thermal annealing enhances the crystallinity of the polymer and improves hole transport. PCDTBT, on the other hand, has only limited short-range order. Its π–π stacking is oriented predominantly normal to the plane of the substrate, and thermal annealing results in a reduction in the coherence of this packing. Because of this decrease in order, thermal annealing worsens hole transport in the out-of-plane direction. Hole-only currents in PCDTBT devices are best described by a model of space-charge limited current that incorporates an exponential distribution of traps, the energetic depth of which increases when the polymer is thermally annealed. These hole-traps may limit optimal PCDTBT-based BHJs to thicknesses that are too thin to absorb all of the above band gap light.

The importance of traps in PCDTBT/$PC_{70}BM$ BHJs suggests a recombination mechanism that was not often considered during study of P3HT based BHJs. The difference in recombination mechanisms may account for the finding that for sufficiently thin films, PCDTBT/$PC_{70}BM$ BHJs can achieve near 100% charge collection efficiency, while P3HT-based devices cannot for any thickness. Recombination due to carrier trapping is not often considered in polymer BHJs, except in those using non-fullerene acceptors,[59,60] because it is not believed to be the dominant loss mechanism in the "fruit-fly" P3HT system. Nevertheless, increasing the power conversion efficiency of

PCDTBT based BHJs by using optically thick films will necessitate a reduction in the density or energetic depth of hole-traps in the polymer. This suggests that P3HT is not prototypical of the new class of high efficiency polymers and that further improvement of BHJ efficiencies will necessitate the study of high efficiency polymers with low structural order.

4. Experimental Section

The substrate preparation for solar cells and hole-only devices was identical. Glass coated with patterned tin-doped indium oxide (ITO, 15 Ω/sq.) was scrubbed and cleaned in an ultrasonic bath of diluted Extran 300 for ~15 minutes. After being rinsed in de-ionized water, the substrates were put in ultrasonic baths of acetone and then isopropyl alcohol for ~10 minutes each. They were dried with nitrogen then were put in a UV-ozone plasma for ~15 minutes. An aqueous solution of poly(3,4-ethylenedioxythiophene) poly(styrenesulfonate) (PEDOT, CLEVIOS P VP AI 4083, work function ~5.0 eV), was spun on top, then baked on a hotplate for ~15 minutes at 140 °C to drive off any remaining solvent, resulting in a film with thickness ~25 nm. The substrates were then transferred to a dry nitrogen glove box for the active layer deposition.

Active layer solutions were prepared in the glove box by dissolving a 1:4 weight ratio of PCDTBT (St. Jean Photochemicals, M_w = 112 kDa), and $PC_{70}BM$ (Nano C) in 1,2-*ortho*-dichlorobenze. The solutions were stirred overnight at 90 °C then cooled to 60 °C for the active layer to be deposited by spin coating. Active layer thicknesses were controlled by varying the solution concentration (9 mg mL^{-1} for pure PCDTBT solutions, and 25–40 mg mL^{-1} total solute for PCDTBT/$PC_{70}BM$ blends) and spin speed (700–1500 rpm). Spin times were generally 45 s, however in the case of the thickest films, the spin time was decreased to 5–7 s to increase film thickness. All films were allowed to dry slowly in covered petri dishes at room temperature. Annealing was performed on a hot plate in the glove box following the complete drying of the active layer and before deposition of the top electrodes. Unless specified otherwise, all annealing times were 10 minutes. For PCDTBT/$PC_{70}BM$ solar cells, a top electrode of 7 nm Ca followed by ~200 nm of Al was deposited by thermal evaporation at a background pressure of ~1×10^{-6} torr. For hole-only devices, a top contact of CA-1914 (Plextronics, diluted by 50% in ethanol, work function ~5.5 eV) was spin-cast in air, and the remaining solvent was driven off by heating on a hotplate at 65 °C for 15 minutes. Following deposition of the CA-1914, the hole-only devices were returned to the glove box where ~200 nm of Al was deposited by thermal evaporation. Hole-only devices were also made using high work-function metal and metal-oxide electrodes in place of a CA-1914 layer. Devices made in this way were not removed from the glove box at any point following substrate preparation, and their hole-transport characteristics were similar to those made with CA-1914. The area for all solar cell and hole-only devices was 0.1 cm^2.

Solar cell current-voltage and EQE measurements were all carried out in the glove box. Current-voltage characteristics were obtained using a Keithley 2400 source meter and a Spectra-Physics 91160-1000 solar simulator, which was calibrated to 1 sun (AM 1.5 G) with an NREL certified KG-5 filtered silicon photodiode. EQE was measured by the method described in the body of the text. The white light bias was calibrated to 1 sun (AM 1.5G) using the same KG-5 filtered silicon photodiode as was used for solar cell measurements.

Current-voltage characteristics for hole-only devices were measured in an evacuated, liquid nitrogen cooled Janus ST-100 cryostat using a Keithley 2400 source meter. Devices were loaded into the cryostat in the glove box prior to measurement to avoid exposure to air. Film thicknesses were measured separately for each device using a Veeco Dektak profilometer. The voltages shown in plots of hole-only current measurements were corrected for the potential lost due to series resistance, $V = V_{applied} - IR_{series}$. They were not corrected for any built-in potential due to a difference in electrode work functions, because in the measurement range (3 V–15 V) this correction is small, and the actual built in voltage is not necessarily the difference in nominal electrode work functions.

Films used for GIXS were prepared on silicon wafers coated with ~25 nm PEDOT (CLEVIOS P VP AI 4083) and were deposited by spin coating using the same solutions as was used for solar cells and hole-only devices. Measurements were performed at the Stanford Synchrotron Radiation Lightsource, Beamline 11-3 with a photon wavelength of 0.09758 nm and an incidence angle of 0.12°. Images were analyzed using the software package WxDiff, which was developed by Dr. Stefan Mannsfeld.[61] Cake segments along the meridian were obtained by integrating GIXS intensities from 80° to 100°, and were used to increase the signal to noise ratio over that of a pure line cut along a 90° line. The cake segments were fit with a superposition of two pseudo-Voigt peaks (centered at 1.30 $Å^{-1}$ and 1.58 $Å^{-1}$) and a constant background. Standard errors for L_{coh} (Figure 3) were calculated by propagating the uncertainty the measurement of scattering intensities. Line cuts along the q_{xy} direction were taken at q_z = 0.02 $Å^{-1}$ with no integration along q_z or the polar angle, and were fit with a superposition of pseudo-Voigt peaks with the same centers as the out-of-plane cake segments and an exponentially increasing background.

Samples for photoluminescence measurements were prepared on cleaned glass substrates with films deposited by spin coating as described above. The samples were excited with an Ar ion laser (λ = 488 nm) and the photoluminescence spectra were captured using a Princeton Instruments spectrophotometer. Photoluminescence signals were normalized for the optical absorption of the film at the excitation wavelength, which was measured using an Ocean Optics DT-1000-CE UV-Vis spectrometer.

Acknowledgements

The authors would like to thank Dr. Suzana Nunes for her helpful discussions of polymer morphology. PCDTBT was provided by St. Jean Photochemicals and CA-1914 by Plextronics. This work was supported by the Center for Advanced Molecular Photovoltaics (CAMP) (Award No KUS-C1-015-21) made by the King Abdullah University of Science and Technology (KAUST). Additional funding was provided by the National Defense Science and Engineering Graduate (NDSEG) Fellowship (Z.M.B.) and the Fannie and John Hertz Foundation (E.T.H.). Portions of this research were carried out at the Stanford Synchrotron Radiation Lightsource user facility, operated by Stanford University on behalf of the U.S. Department of Energy, Office of Basic Energy Sciences.

Received: April 13, 2011
Revised: June 3, 2011
Published online:

[1] V. Kamm, G. Battagliarin, I. A. Howard, W. Pisula, A. Mavrinskiy, C. Li, K. Müllen, F. Laquai, *Adv. Energy Mater.* **2011**, *1*, 297.
[2] C. J. Brabec, S. Gowrisanker, J. J. M. Halls, D. Laird, S. Jia, S. P. Williams, *Adv. Mater.* **2010**, *22*, 3839.
[3] H.-Y. Chen, J. Hou, S. Zhang, Y. Liang, G. Yang, Y. Yang, L. Yu, Y. Wu, G. Li, *Nat. Photonics* **2009**, *3*, 649.
[4] T.-Y. Chu, J. Lu, S. Beaupré, Y. Zhang, J.-R. Pouliot, S. Wakim, J. Zhou, M. Leclerc, Z. Li, J. Ding, Y. Tao, *J. Am. Chem. Soc.* **2011**, *133*, 4250.
[5] Y. Liang, Z. Xu, J. Xia, S.-T. Tsai, Y. Wu, G. Li, C. Ray, L. Yu, *Adv. Mater.* **2010**, *22*, E135.
[6] J. Peet, J. Y. Kim, N. E. Coates, W. L. Ma, D. Moses, A. J. Heeger, G. C. Bazan, *Nat. Mater.* **2007**, *6*, 497.
[7] C. Piliego, T. W. Holcombe, J. D. Douglas, C. H. Woo, P. M. Beaujuge, J. M. J. Fréchet, *J. Am. Chem. Soc.* **2010**, *132*, 7595.
[8] S. C. Price, A. C. Stuart, L. Yang, H. Zhou, W. You, *J. Am. Chem. Soc.* **2011**, *133*, 4625.

[9] Y. Sun, C. J. Takacs, S. R. Cowan, J. H. Seo, X. Gong, A. Roy, A. J. Heeger, *Adv. Mater.* **2011**, *23*, 2226.
[10] S. H. Park, A. Roy, S. Beaupré, S. Cho, N. Coates, J. S. Moon, D. Moses, M. Leclerc, K. Lee, A. J. Heeger, *Nat. Photonics* **2009**, *3*, 297.
[11] C. H. Peters, I. T. Sachs-Quintana, J. P. Kastrop, S. Beaupré, M. Leclerc, M. D. McGehee, *Adv. Energy Mater.* **2011**, doi: 10.1002/aenm.201100138.
[12] G. F. Burkhard, E. T. Hoke, S. R. Scully, M. D. McGehee, *Nano Lett.* **2009**, *9*, 4037.
[13] V. D. Mihailetchi, H. Xie, B. de Boer, L. J. A. Koster, P. W. M. Blom, *Adv. Funct. Mater.* **2006**, *16*, 699.
[14] S. Cho, J. H. Seo, S. H. Park, S. Beaupré, M. Leclerc, A. J. Heeger, *Adv. Mater.* **2010**, *22*, 1253.
[15] E. Verploegen, R. Mondal, C. J. Bettinger, S. Sok, M. F. Toney, Z. Bao, *Adv. Funct. Mater.* **2010**, *20*, 3519.
[16] N. Blouin, A. Michaud, M. Leclerc, *Adv. Mater.* **2007**, *19*, 2295.
[17] S. Lilliu, T. Agostinelli, E. Pires, M. Hampton, J. Nelson, J. E. MacDonald, *Macromolecules* **2011**, doi: 10.1021/ma102817z.
[18] Y. Kim, S. Cook, S. M. Tuladhar, S. A. Choulis, J. Nelson, J. R. Durrant, D. D. C. Bradley, M. Giles, I. McCulloch, C.-S. Ha, M. Ree, *Nat. Mater.* **2006**, *5*, 197.
[19] H. Sirringhaus, P. J. Brown, R. H. Friend, M. M. Nielsen, K. Bechgaard, B. M. W. Langeveld-Voss, A. J. H. Spiering, R. A. J. Janssen, E. W. Meijer, P. Herwig, D. M. de Leeuw, *Nature* **1999**, *401*, 685.
[20] M. L. Chabinyc, M. F. Toney, R. J. Kline, I. McCulloch, M. Heeney, *J. Am. Chem. Soc.* **2007**, *129*, 3226.
[21] J. Rivnay, R. Noriega, J. E. Northrup, R. J. Kline, M. F. Toney, A. Salleo, *Phys. Rev. B* **2011**, *83*, 121306(R).
[22] I. McCulloch, M. Heeney, C. Bailey, K. Genevicius, I. MacDonald, M. Shkunov, D. Sparrowe, S. Tierney, R. Wagner, W. Zhang, M. L. Chabinyc, R. J. Kline, M. D. McGehee, M. F. Toney, *Nat. Mater.* **2006**, *5*, 328.
[23] M. A. Lampert, P. Mark, *Current Injection in Solids*, Academic Press, New York **1970**.
[24] H. Bässler, *Phys. Status Solidi B* **1993**, *175*, 15.
[25] S. V. Novikov, D. H. Dunlap, V. M. Kenkre, P. E. Parris, A. V. Vannikov, *Phys. Rev. Lett.* **1998**, *81*, 4472.
[26] W. F. Pasveer, J. Cottaar, C. Tanase, R. Coehoorn, P. A. Bobbert, P. W. M. Blom, D. M. de Leeuw, M. A. J. Michels, *Phys. Rev. Lett.* **2005**, *94*, 206601.
[27] E. Murphy, R. Good Jr., *Phys. Rev.* **1956**, *102*, 1464.
[28] P. Mark, W. Helfrich, *J. Appl. Phys.* **1962**, *33*, 205.
[29] P. W. M. Blom, M. J. M. de Jong, J. J. M. Vleggaar, *Appl. Phys. Lett.* **1996**, *68*, 3308.
[30] M. M. Mandoc, B. de Boer, G. Paasch, P. W. M. Blom, *Phys. Rev. B* **2007**, *75*, 193202.
[31] Y. Zhang, B. de Boer, P. W. M. Blom, *Phys. Rev. B* **2010**, *81*, 085201.
[32] M. M. Mandoc, B. de Boer, P. W. M. Blom, *Phys. Rev. B* **2006**, *73*, 155205.
[33] S. L. M. van Mensfoort, R. J. de Vries, V. Shabro, H. Loebl, R. A. J. Janssen, R. Coehoorn, *Org. Electron.* **2010**, *11*, 1408.
[34] S. L. M. van Mensfoort, J. Billen, S. I. E. Vulto, R. A. J. Janssen, R. Coehoorn, *Phys. Rev. B* **2009**, *80*, 033202.
[35] A. J. Campbell, D. D. C. Bradley, D. G. Lidzey, *J. Appl. Phys.* **1997**, *82*, 6326.
[36] Z. Chiguvare, V. Dyakonov, *Phys. Rev. B* **2004**, *70*, 235207.
[37] D. S. Chung, D. H. Lee, C. Yang, K. Hong, C. E. Park, J. W. Park, S.-K. Kwon, *Appl. Phys. Lett.* **2008**, *93*, 033303.
[38] G. Juška, K. Arlauskas, M. Viliūnas, J. Kočka, *Phys. Rev. Lett.* **2000**, *84*, 4946.
[39] J. Lorrmann, B. H. Badada, O. Inganas, V. Dyakonov, C. Deibel, *J. Appl. Phys.* **2010**, *108*, 113705.
[40] L. J. A. Koster, E. C. P. Smits, V. D. Mihailetchi, P. W. M. Blom, *Phys. Rev. B* **2005**, *72*, 085205.
[41] D. Monroe, *Phys. Rev. Lett.* **1985**, *54*, 146.
[42] J. Cornil, D. Beljonne, J.-P. Calbert, J.-L. Brédas, *Adv. Mater.* **2001**, *13*, 1053.
[43] H. Bässler, *Phys. Status Solidi B* **1981**, *107*, 9.
[44] X. Yang, J. Loos, S. C. Veenstra, W. J. H. Verhees, M. M. Wienk, J. M. Kroon, M. A. J. Michels, R. A. J. Janssen, *Nano Lett.* **2005**, *5*, 579.
[45] S. M. Tuladhar, D. Poplavskyy, S. A. Choulis, J. R. Durrant, D. D. C. Bradley, J. Nelson, *Adv. Funct. Mater.* **2005**, *15*, 1171.
[46] N. C. Cates, R. Gysel, J. E. P. Dahl, A. Sellinger, M. D. McGehee, *Chem. Mater.* **2010**, *22*, 3543.
[47] C. Melzer, E. J. Koop, V. D. Mihailetchi, P. W. M. Blom, *Adv. Funct. Mater.* **2004**, *14*, 865.
[48] C. Deibel, A. Wagenpfahl, V. Dyakonov, *Phys. Rev. B* **2009**, *80*, 075203.
[49] R. A. Street, M. Schoendorf, A. Roy, J. H. Lee, *Phys. Rev. B* **2010**, *81*, 205307.
[50] M. Tong, N. E. Coates, D. Moses, A. J. Heeger, S. Beaupré, M. Leclerc, *Phys. Rev. B* **2010**, *81*, 125210.
[51] C. Deibel, A. Wagenpfahl, *Phys. Rev. B* **2010**, *82*, 207301.
[52] R. A. Street, *Phys. Rev. B* **2010**, *82*, 207302.
[53] Z. Li, C. McNeill, *J. Appl. Phys.* **2011**, *109*, 074513.
[54] H. Field, *National Center for Photovoltaics Program Review Meeting* **1998**.
[55] X. Yang, J. van Duren, R. A. J. Janssen, M. A. J. Michels, J. Loos, *Macromolecules* **2004**, *37*, 2151.
[56] A. C. Mayer, M. F. Toney, S. R. Scully, J. Rivnay, C. J. Brabec, M. Scharber, M. Koppe, M. Heeney, I. McCulloch, M. D. McGehee, *Adv. Funct. Mater.* **2009**, *19*, 1.
[57] N. C. Cates, R. Gysel, Z. Beiley, C. E. Miller, M. F. Toney, M. Heeney, I. McCulloch, M. D. McGehee, *Nano Lett.* **2009**, *9*, 4153.
[58] N. C. Miller, R. Gysel, C. E. Miller, E. Verploegen, Z. Beiley, M. Heeney, I. McCulloch, Z. Bao, M. F. Toney, M. D. McGehee, *J. Polym. Sci. Pol. Phys.* **2011**, *49*, 499.
[59] M. M. Mandoc, W. Veurman, L. J. A. Koster, M. M. Koetse, J. Sweelssen, B. de Boer, P. W. M. Blom, *J. Appl. Phys.* **2007**, *101*, 104512.
[60] C. R. McNeill, I. Hwang, N. C. Greenham, *J. Appl. Phys.* **2009**, *106*, 024507.
[61] S. Mannsfeld, wxdiff: Diffraction image processing and data analysis software, http://code.google.com/p/wxdiff/(January, 2011).